analytical chemistry

pubs.acs.org/ac Article

Highly Stable Covalent Organic Framework Nanosheets as a New Generation of Electrochemiluminescence Emitters for Ultrasensitive MicroRNA Detection

Jin-Ling Zhang, Yang Yang, Wen-Bin Liang, Li-Ying Yao, Ruo Yuan,* and Dong-Rong Xiao*

Cite This: *Anal. Chem.* 2021, 93, 3258−3265 Read Online

ACCESS | Metrics & More | Article Recommendations | Supporting Information

ABSTRACT: A pyrene-based sp^2 carbon-conjugated covalent organic framework (COF) nanosheet (Py-sp^2c-CON) with strong and stable electrochemiluminescence (ECL) emission was constructed by C═C polycondensation of tetrakis(4-formylphenyl)pyrene (TFPPy) and 2,2′-(1,4-phenylene)-diacetonitrile, which was employed as a highly efficient ECL emitter to fabricate an ECL biosensor for the first time. The Py-sp^2c-CON exhibited higher ECL intensity and efficiency than those of TFPPy, bulk Py-sp^2c-COF, and imine-linked pyrene COF, not only because the pyrene luminophores and aggregation-induced emissive luminogens (cyano-substituted phenylenevinylene) were topologically linked into Py-sp^2c-CON, which greatly increased the immobilization amount of luminophores and decreased the aggregation-caused quenching effect and nonradiative transition but also because the porous ultrathin structure of Py-sp^2c-CON effectively shortened transport distances of an electron, ion, and co-reactant ($S_2O_8^{2-}$), which made more ECL luminophores be activated and thus efficiently increased the utilization ratio of luminophores. More interestingly, when Bu_4NPF_6 was introduced into the Py-sp^2c-CON/$S_2O_8^{2-}$ system as a co-reaction accelerator, the ECL signal of Py-sp^2c-CON was further amplified. As expected, the average ECL intensity of the Py-sp^2c-CON/$S_2O_8^{2-}$/Bu_4NPF_6 system was about 2.03, 5.76, 24.31, and 190.33-fold higher than those of Py-sp^2c-CON/$S_2O_8^{2-}$, Py-sp^2c-COF/$S_2O_8^{2-}$, TFPPy/$S_2O_8^{2-}$ and imine-linked pyrene COF/$S_2O_8^{2-}$ systems. Considering these advantages, the Py-sp^2c-CON/$S_2O_8^{2-}$/Bu_4NPF_6 system was employed to prepare an ECL biosensor for microRNA-21 detection, which exhibited a broad linear response (100 aM to 1 nM) and a low detection limit (46 aM). Overall, this work demonstrated that sp^2 carbon CONs can be directly used as a high-performance ECL emitter, thus expanding the application scope of COFs and opening a new horizon to develop new types of ECL emitters.

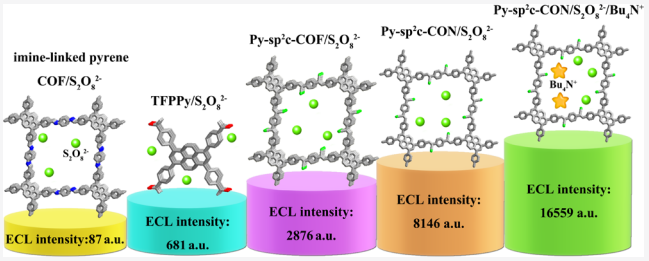

INTRODUCTION

MicroRNA-21 (miRNA-21) has attracted widespread attention in recent years because it is regarded as a biomarker of various cancers, including lung cancer, stomach cancer, prostate cancer, and pancreas cancer.[1,2] Therefore, the establishment of a simple, rapid, and ultrasensitive method for miRNA-21 detection is vitally important for the early diagnosis of cancers.[3] So far, a variety of methods have been developed for miRNA-21 analysis, such as Raman,[4] electrochemistry,[5] chemiluminescence,[6] fluorescence,[7] and electrochemiluminescence (ECL).[8] Among these methods, ECL is a particularly excellent detection method owing to its high sensitivity, good controllability, and a near-zero background signal.[9] However, owing to the intrinsic features of miRNAs, including small size, low concentration, and analogical sequences in family members, it is still a challenge to sensitively detect miRNA-21 in clinical diagnosis.[10] Thus, searching for an effective way to enhance the ECL intensity and increase the sensitivity of an ECL sensor is very significant for miRNA-21 detection. Recently, in order to increase the ECL signal, various nanomaterials, such as carbon nanotubes (CNTs),[11] silica nanoparticles (NPs),[12] graphene oxide (GO),[13] and metal−organic frameworks (MOFs),[14] have been used as carriers to immobilize ECL luminophores. Among them, MOFs have attracted enormous research interest in recent years owing to their permanent pore architecture and very high surface areas, which could vastly enhance the loading capacity of ECL luminophores.[15,16] However, owing to the poor stability of most MOFs in water, the leaching of ECL luminophores during experiments may seriously affect the stability of an ECL sensor.[17,18] Moreover, most of the reported MOF-based ECL materials were constructed from the introduction of Ru(II) complexes into MOFs by encapsulation, doping, or post-

Received: November 23, 2020
Accepted: January 22, 2021
Published: February 2, 2021

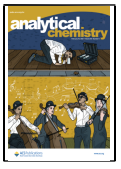

https://dx.doi.org/10.1021/acs.analchem.0c04931
Anal. Chem. 2021, 93, 3258−3265

synthetic modification.[19] The costly Ru(II) complexes have potential biotoxicity and large steric hindrance, which limit the immobilized amount of luminophores and hamper the widespread application of MOF-based ECL materials. Therefore, it is urgent and significant to design and construct a new type of stable porous ECL materials with a high immobilized amount of luminophores, inexpensive cost, and good biocompatibility.

Covalent organic frameworks (COFs) are a new class of crystalline porous materials, which are constructed by organic building units via strong covalent bonds.[20,21] Benefitting from their structural tunability, well-ordered porosity, ultrahigh surface areas, high chemical stability, and low density,[22] COFs have shown potential applications in many fields including ion transport, catalysis, gas storage, drug delivery, and sensing.[23,24] Compared with MOFs, most COFs have better water stability owing to the strong covalent bonds.[25] Furthermore, COFs are a class of metal-free materials and thus possess superior biocompatibility and low biotoxicity.[26] Therefore, the chemically stable COFs are ideal candidate materials for the fabrication of highly stable and ultrasensitive sensors. Recently, COFs have been used to fabricate various sensors, such as a chemical sensor,[27] humidity sensor,[28] and a colorimetric pH sensor.[29] In contrast, the study of COF-based ECL sensors is still in its infancy. Till now, only one ECL sensor based on $Ru(bpy)_3^{2+}$@COF-LZU1 has been reported.[30] However, directly using COFs as ECL emitters to construct ECL sensors has never been reported. The reason might be that the ubiquitous strong $\pi-\pi$ stacking interactions in COFs can easily trigger the aggregation-caused quenching (ACQ) effect, which reduces the luminescence efficiency of COFs and thus leads to less or non-emissive COFs.[31] Moreover, the most common COFs are connected by imine bonds; the rotationally labile imine linkages cause the nonradiative transition, which further decreases the luminescence efficiency of the imine-linked COFs.[27,32] In 2001, Tang's group discovered the aggregation-induced emission (AIE) effect, which provided an efficient strategy to solve the ACQ problem and lighted up a lamp for designing solid-state materials with high luminescence efficiency.[33,34] More recently, Tang et al. reported some examples of attaching AIE luminogens (AIEgens) to traditional planar ACQ luminophores with the aim of reducing the ACQ effect of the planar luminophores and achieving ACQ-to-AIE transformation.[35−38] Inspired by the above studies, we speculated that it should be feasible to construct high-performance COF-based ECL materials by topologically connecting ACQ luminophores with AIEgens. Based on the abovementioned considerations, we synthesized a highly stable pyrene-based sp^2 carbon-conjugated COF (Py-sp^2c-COF) via C═C polycondensation of tetrakis(4-formylphenyl)pyrene (TFPPy) and 2,2′-(1,4-phenylene)diacetonitrile (PDAN) (Scheme 1A). Pyrene (ACQ luminophores) and cyano-substituted phenylenevinylene (AIEgens)[39] were topologically linked together in the Py-sp^2c-COF (Figure S1A), which could efficiently decrease the ACQ effect and increase the loading capacity of ECL luminophores, thereby resulting in a Py-sp^2c-COF with high ECL intensity and efficiency. However, because the electrochemical activation of the interior ECL luminophores was restrained by the long transportation path of the ions, electrons, co-reactants, and co-reactant intermediates in a three-dimensional (3D) bulk Py-sp^2-COF, the utilization ratio of the ECL luminophores was still limited. To improve the utilization ratio of the luminophores and further enhance the

Scheme 1. (A) Synthesis of Py-sp^2c-CON; (B) the Exo III-Assisted Target Recycling Amplification Reaction; (C) the Fabrication Procedures of the ECL Biosensor

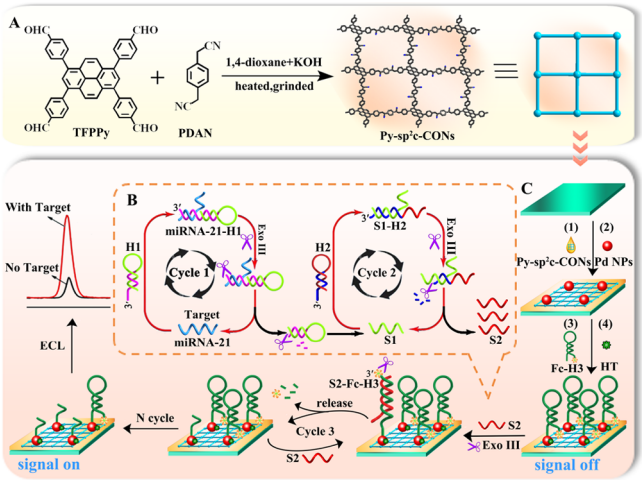

ECL intensity, ultrathin covalent organic nanosheets (CONs) with a shortened transportation path of ions, electrons, co-reactants, and co-reactant intermediates are greatly needed. Therefore, the 3D bulk Py-sp^2c-COF was ground into ultrathin Py-sp^2c-CON.[40] Compared with the 3D bulk Py-sp^2c-COF, the ultrathin Py-sp^2c-CON effectively improves the utilization ratio of ECL luminophores, thereby exhibiting higher ECL intensity. More interestingly, when Bu_4NPF_6 was added to the Py-sp^2c-CON/$S_2O_8^{2-}$ system as a co-reaction accelerator, which could catalyze the reduction of co-reactant $S_2O_8^{2-}$ to produce more $SO_4^{\cdot-}$, the ECL signal of Py-sp^2c-CON was further enhanced. As expected, under the same experimental conditions, it was found that the average ECL intensity of the Py-sp^2c-CON/$S_2O_8^{2-}$/Bu_4NPF_6 system was around 2.03, 5.76, 24.31, and 190.33 times those of Py-sp^2c-CON/$S_2O_8^{2-}$, 3D bulk Py-sp^2c-COF/$S_2O_8^{2-}$, TFPPy/$S_2O_8^{2-}$, and imine-linked pyrene COF/$S_2O_8^{2-}$ systems. Moreover, the Py-sp^2c-CON/$S_2O_8^{2-}$/Bu_4NPF_6 system also exhibited higher ECL efficiency than those of Py-sp^2c-CON/$S_2O_8^{2-}$, 3D bulk Py-sp^2c-COF/$S_2O_8^{2-}$, and TFPPy/$S_2O_8^{2-}$ systems. What is even more impressive is that Py-sp^2c-CON still possesses a strong and stable ECL emission after being dispersed in water for 6 months owing to its excellent stability in water.

Considering the abovementioned excellent ECL performance, an ultrasensitive "off−on" ECL biosensor based on the Py-sp^2c-CON/$S_2O_8^{2-}$/Bu_4NPF_6 system and an exonuclease III (Exo III)-assisted target recycling amplification strategy was proposed for the determination of miRNA-21. The principle of this sensing strategy is shown in Scheme 1B,C. Initially, the Py-sp^2c-CON was dripped on the electrode surface to form a uniform film. After that, the palladium NPs (Pd NPs) were bedecked on the modified electrode for further assembling the ferrocene-labeled H3 (Fc-H3), which quenched the ECL emission of Py-sp^2c-CON through Fc groups ("signal-off" state, Scheme 1C). Meanwhile, as shown in Scheme 1B, the target miRNA-21 could specifically recognize the 3′-protruding DNA fragment of hairpin H1 and hybridize with it to form an miRNA-21-H1 complex with blunt 3′-terminus. Subsequently, the miRNA-21-H1 complex was digested by Exo III to liberate the target miRNA-21 for recycle (cycle 1) and produce numerous new DNA fragments (secondary target DNA fragment, S1) for initiating the next cycle (cycle 2). Then S1

https://dx.doi.org/10.1021/acs.analchem.0c04931
Anal. Chem. 2021, 93, 3258−3265

could open and hybridize with the 3′-protruding DNA fragment of hairpin H2 through the toehold-mediated strand displacement reaction (SDR) to form a new duplex DNA (denoted as S1-H2), which was again cleaved by Exo III, thus releasing both S1 for the cycle 2 process and vast simulated target S2. When the simulated target S2 was added on the surface of the modified electrode, S2 spontaneously hybridized with hairpin Fc-H3 to form duplex DNA (denoted as S2-Fc-H3) with blunt 3′-terminus. Also, with the aid of Exo III, the Fc-H3 in S2-Fc-H3 was cleaved and released from the modified electrode surface. At the same time, the simulated target S2 was released and then combined with the next hairpin Fc-H3 to participate in cycle 3. After multiple cycles, a large amount of Fc-H3 was left from the electrode surface, resulting in a "signal on" state. Therefore, the ECL signal of the sensor increased correspondingly with the increase of the target miRNA-21 concentration. Because of the combination of the excellent ECL performance of the Py-sp^{2}c-CON/$S_2O_8^{2-}$/Bu_4NPF_6 system and the highly efficienct Exo III-assisted target recycling amplification strategy, the proposed biosensor accomplished supersensitive and highly selective detection of miRNA-21. Significantly, this work used highly stable ultrathin Py-sp^{2}c-CON to increase ECL efficiency and intensity, which provided a new conception for the design and preparation of high-performance ECL emitters. Therefore, it opened new perspectives for constructing highly stable and supersensitive ECL sensors and broadened the application scope of COFs.

EXPERIMENTAL SECTION

Synthesis of a Py-sp^{2}c-COF. A Py-sp^{2}c-COF was synthesized according to previous literature with some modification.[41] TFPPy (24 μmol) (15.0 mg), 7.5 mg of PDAN (48 μmol), 1,4-dioxane (1 mL), and 0.1 mL of NaOH (4 M) were mixed in a 10 mL Pyrex tube. The mixture was sonicated for 10 min and degassed three times through a freeze-pump-thaw technique. Then, the Pyrex tube was vacuum sealed and heated to 90 °C for 3 days. The mixture was cooled to room temperature, and the resulting suspension was collected by centrifugation, washed several times with H_2O and THF, respectively, soxhlet extracted in THF for 24 h, and dried under vacuum at 120 °C for 12 h to obtain a Py-sp^{2}c-COF.

Synthesis of Py-sp^{2}c-CON. First, the bulk Py-sp^{2}c-COF was thoroughly ground in an agate mortar. Then, the ground Py-sp^{2}c-COF was dispersed into water, sonicated for 12 h, and centrifuged at 3000 rpm for 3 min to collect the upper solution of Py-sp^{2}c-CON.

Procedure of Biosensor Preparation and ECL Detection. First, each glassy carbon electrode (GCE) was pretreated with the previous method.[42] Next, the prepared Py-sp^{2}c-CON (10 μL) was deposited on the GCE surface and dried at 37 °C to form a uniform film. After decorating 7 μL of Pd NPs on the Py-sp^{2}c-CON/GCE, the modified GCE was incubated with 10 μL of Fc-H3 (4.0 μM) at 4 °C for 12 h. Then, the Fc-H3/Pd NPs/Py-sp^{2}c-CON/GCE was incubated with 10 μL of hexanethiol (HT, 1.0 mM, ethanol) for 1 h to block the nonspecific sites. Following that, the HT/Fc-H3/Pd NPs/Py-sp^{2}c-CON/GCE was incubated with 10 μL of a mixture including various concentrations of S2 and 10 U Exo III at 37 °C for 1.5 h. It is worth mentioning that the modified GCE should be gently rinsed with ultrapure water after every modified step. Finally, the above modified GCEs were placed in 2 mL of phosphate buffered solution (PBS) containing 15 mM $S_2O_8^{2-}$ and 1 mM Bu_4NPF_6 for miRNA-21 detection.

RESULTS AND DISCUSSION

Characterization of Py-sp^{2}c-CON. To confirm the successful synthesis of Py-sp^{2}c-CON, various analytical methods were utilized. The IR spectra of Py-sp^{2}c-CON and the Py-sp^{2}c-COF (Figure S2c,d) are similar and both exhibit a new peak at 2220 cm^{-1} assigned to the cyano side group, and a greatly decreased peak at 2720 cm^{-1} attributed to the C−H bond of the aldehyde group, thus demonstrating the formation of C═C bonds in Py-sp^{2}c-CON and the Py-sp^{2}c-COF. The transmission electron microscopy (TEM) images indicated that Py-sp^{2}c-CON exhibited the ultrathin nanosheet morphology (Figure 1A,B). Meanwhile, the atomic force microscopy

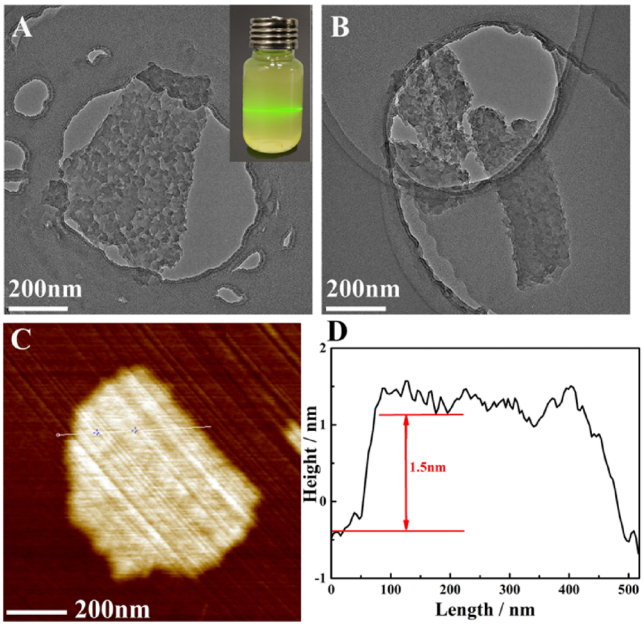

Figure 1. (A, B) TEM images of Py-sp^{2}c-CON; (C, D) AFM image and the height profile of Py-sp^{2}c-CON. Inset of A: the Tyndall effect of Py-sp^{2}c-CON suspension in water.

(AFM) images (Figure 1C,D and Figure S4A−D) further proved that the Py-sp^{2}c-CON possessed nanosheet structures with thickness ranging from 1.5 to 3.8 nm, corresponding to 4−10 layers. Moreover, a typical Tyndall effect can be observed in the suspension of the Py-sp^{2}c-CON (the inset of Figure 1A), verifying their colloidal structure.

Possible ECL Mechanism of the Py-sp^{2}c-CON/$S_2O_8^{2-}$/Bu_4NPF_6 System. To explore the possible ECL reaction mechanism of the Py-sp^{2}c-CON/$S_2O_8^{2-}$/Bu_4NPF_6 system, the ECL of Py-sp^{2}c-CON-modified glassy carbon electrode (Py-sp^{2}c-CON/GCE) was measured in different solutions with the potential scan changing from −2 to 0 V. When the Py-sp^{2}c-CON/GCE was measured in PBS, an extremely low ECL signal was gained (Figure 2A, curve a). After introducing Bu_4NPF_6 to the PBS, the ECL intensity had no obvious difference with that in PBS (Figure 2A, curve b), revealing that Bu_4NPF_6 has no enhancement effect on ECL intensity of Py-sp^{2}c-CON with no co-reactant. When the Py-sp^{2}c-CON/GCE was tested in $S_2O_8^{2-}$/PBS, the ECL intensity increased to 8146 a.u. because $S_2O_8^{2-}$ acted as a co-reactant to promote the ECL emission of Py-sp^{2}c-CON (Figure 2A, curve c). When

https://dx.doi.org/10.1021/acs.analchem.0c04931
Anal. Chem. 2021, 93, 3258−3265

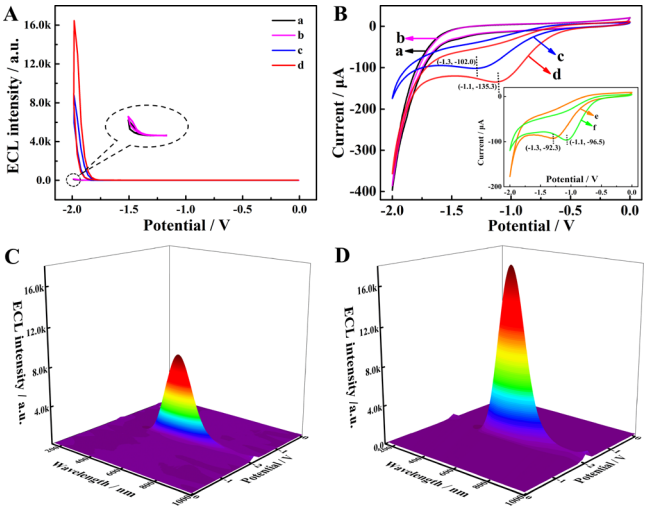

Figure 2. (A) ECL intensities of a Py-sp^{2}c-CON/GCE in PBS solution (a), PBS containing 1 mM Bu_4NPF_6 solution (b), PBS containing 15 mM $S_2O_8^{2-}$ solution (c), and PBS containing 15 mM $S_2O_8^{2-}$ and 1 mM Bu_4NPF_6 solution (d). (B) CV waves of the Py-sp^{2}c-CON/GCE in PBS solution (a), PBS containing 1 mM Bu_4NPF_6 solution (b), PBS containing 15 mM $S_2O_8^{2-}$ solution (c), and PBS containing 15 mM $S_2O_8^{2-}$ and 1 mM Bu_4NPF_6 solution (d). Inset of B: the CV waves of the bare GCE in PBS containing 15 mM $S_2O_8^{2-}$ solution (e) and PBS containing 15 mM $S_2O_8^{2-}$ solution and 1 mM Bu_4NPF_6 solution (f). 3D ECL spectra of the Py-sp^{2}c-CON/GCE in (C) PBS containing 15 mM $S_2O_8^{2-}$ solution and (D) PBS containing 15 mM $S_2O_8^{2-}$ and 1 mM Bu_4NPF_6 solution.

Bu_4NPF_6 was introduced in the $S_2O_8^{2-}$/PBS, the ECL intensity notably increased to 16559 a.u. (Figure 2A, curve d). Combining the mechanism of the co-reaction accelerator with our experimental results,[43] we preliminarily inferred that the Bu_4NPF_6 as a co-reaction accelerator could obviously increase the ECL emission of Py-sp^{2}c-CON by catalyzing the electrochemical reduction of $S_2O_8^{2-}$ to generate vast $SO_4^{\cdot-}$.

To verify the supposition, the cyclic voltammetry (CV) curves of different modified electrodes were gained from −2 V to 0 V. When the bare GCE was measured in $S_2O_8^{2-}$/Bu_4NPF_6/PBS, the reduction peak current increased obviously and the peak potential shifted positively (−1.1 V, −96.5 μA, the inset of Figure 2B, curve f) in comparison to that in $S_2O_8^{2-}$/PBS (−1.3 V, −92.3 μA, the inset of Figure 2B, curve e), suggesting more $S_2O_8^{2-}$ was reduced in the process. Furthermore, the CV curve of the Py-sp^{2}c-CON/GCE in PBS (Figure 2B, curve a) is similar to that in Bu_4NPF_6/PBS (Figure 2B, curve b), revealing Bu_4NPF_6 did not directly interact with Py-sp^{2}c-CON to enhance the ECL intensity. In addition, the CV curve of the Py-sp^{2}c-CON/GCE in $S_2O_8^{2-}$/Bu_4NPF_6/PBS displayed a more positive potential of −1.1 V and an obviously stronger peak current (−135.3 μA; Figure 2B, curve d) than that in $S_2O_8^{2-}$/PBS (−1.3 V, −102.0 μA; Figure 2B, curve c), suggesting that Bu_4NPF_6 indeed increased the reduction rate of $S_2O_8^{2-}$ and further increased the ECL intensity of the Py-sp^{2}c-CON/$S_2O_8^{2-}$ system.

The ECL spectra were measured to further confirm the above conclusion. The ECL spectrum of the Py-sp^{2}c-CON/$S_2O_8^{2-}$ system displayed the maximum ECL emission peak at 565 nm (Figure 2C; Figure 3, curve blue), which was near to the photoluminescence emission peak at 563 nm (Figure 3, curve red), indicating that the luminophore was the Py-sp^{2}c-CON in the Py-sp^{2}c-CON/$S_2O_8^{2-}$ system. After the Bu_4NPF_6 was added into the Py-sp^{2}c-CON/$S_2O_8^{2-}$ system, the ECL intensity of the Py-sp^{2}c-CON/$S_2O_8^{2-}$ system was improved, but the maximum emission wavelength remained unaltered (Figure 2D), revealing that the luminophore of the Py-sp^{2}c-CON/$S_2O_8^{2-}$/Bu_4NPF_6 system was still Py-sp^{2}c-CON. According to literature[44] and the above experiment results, the possible ECL mechanism of the Py-sp^{2}c-CON/$S_2O_8^{2-}$/Bu_4NPF_6 system could be proposed as the following: eqs 1a−4. In addition the $SO_4^{\cdot-}$ radicals generated from the direct reduction of $S_2O_8^{2-}$ on the electrode surface (eq 1a), Bu_4N^+, could react with $S_2O_8^{2-}$ to accelerate the electrochemical reduction of $S_2O_8^{2-}$ (eq 1b),[45−50] resulting in more $SO_4^{\cdot-}$ radicals per unit time. Thus, the reaction rate between $SO_4^{\cdot-}$ and Py-sp^{2}c-CON$^{\cdot-}$ was significantly increased and led to a remarkable enhancement of ECL emission.

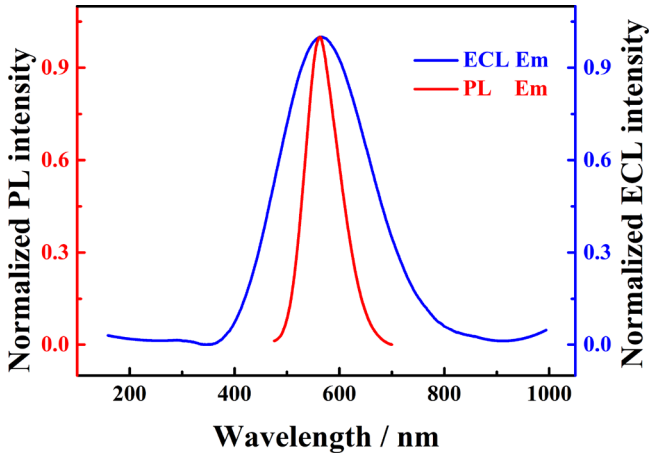

Figure 3. Normalized photoluminescence (PL) emission spectrum (curve red) and ECL emission spectrum (curve blue) of Py-sp^{2}c-CON.

$$S_2O_8^{2-} + e^- \rightarrow SO_4^{2-} + SO_4^{\cdot-} \quad (1a)$$

$$Bu_4N^+ + 2S_2O_8^{2-} + e^- \rightarrow [Bu_3N^{\bullet}]^+ + H^+ + \text{1-butene} + 2SO_4^{2-} + 2SO_4^{\bullet-} \quad (1b)$$

$$Py - sp^2\,c - CON + e^- \rightarrow Py - sp^2\,c - CON^{\cdot-} \quad (2)$$

$$Py - sp^2\,c - CON^{\cdot-} + SO_4^{\cdot-} \rightarrow Py - sp^2\,c - CON^{*} + SO_4^{2-} \quad (3)$$

$$Py - sp^2\,c - CON^{*} \rightarrow Py - sp^2\,c - CON + h\nu \quad (4)$$

ECL Performance of the Py-sp^{2}c-CON/$S_2O_8^{2-}$/Bu_4NPF_6 System. To better understand the excellent ECL performance of the Py-sp^{2}c-CON/$S_2O_8^{2-}$/Bu_4NPF_6 system, the ECL intensities of Py-sp^{2}c-CON/$S_2O_8^{2-}$/Bu_4NPF_6, Py-sp^{2}c-CON/$S_2O_8^{2-}$, 3D bulk Py-sp^{2}c-COF/$S_2O_8^{2-}$, TFPPy/$S_2O_8^{2-}$, and the imine-linked pyrene COF/$S_2O_8^{2-}$ (Figure S1B) systems were compared. As can be figured out from Figure 4A and Figure S7, the 3D bulk Py-sp^{2}c-COF/$S_2O_8^{2-}$ system displayed an average ECL intensity of 2876 a.u. (Figure 4A, curve c), which was superior to those of TFPPy/$S_2O_8^{2-}$ (681 a.u., Figure 4A, curve b and Figure S7) and imine-linked pyrene COF/$S_2O_8^{2-}$ systems (87 a.u., Figure 4A, curve a) under identical conditions. The result was attributed to the following three aspects: First, the olefin-linked Py-sp^{2}c-COF can

https://dx.doi.org/10.1021/acs.analchem.0c04931
Anal. Chem. 2021, 93, 3258−3265

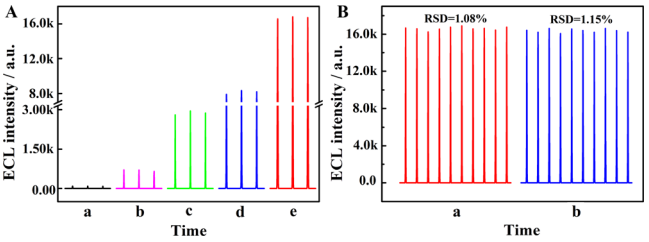

Figure 4. (A) ECL intensities of imine-linked pyrene COF/$S_2O_8^{2-}$ (a), TFPPy/$S_2O_8^{2-}$ (b), 3D bulk Py-sp^{2}c-COF/$S_2O_8^{2-}$ (c), Py-sp^{2}c-CON/$S_2O_8^{2-}$ (d), and Py-sp^{2}c-CON/$S_2O_8^{2-}$/Bu_4NPF_6 (e) systems. (B) ECL intensities of the Py-sp^{2}c-CON/$S_2O_8^{2-}$/Bu_4NPF_6 system before (a) and after (b) treatment in water and stored at 4 °C for 6 months.

effectively avoid the rotation of the imine bond and reduce unnecessary energy loss, and thereby exhibiting highly luminous efficiency. Second, the Py-sp^{2}c-COF was topologically linked by pyrene luminophores and AIEgens (Figure S1A), which could greatly decrease the ACQ effect and increase the loading capacity of ECL luminophores, thereby resulting in the Py-sp^{2}c-COF with high ECL intensity and efficiency. Third, owing to the enrichment of $S_2O_8^{2-}$ in the pores of the Py-sp^{2}c-COF, the distance between ECL luminophores and the co-reactant was shortened, which allowed more internal luminophores to be electrochemically activated and thus further enhanced ECL intensity. When the 2D ultrathin Py-sp^{2}c-CON-modified electrode was tested in PBS containing 15 mM $S_2O_8^{2-}$, the ECL intensity (8146 a.u., Figure 4A, curve d) was obviously stronger than that of the 3D bulk Py-sp^{2}c-COF/$S_2O_8^{2-}$ system. This indicated that 2D ultrathin Py-sp^{2}c-CON can effectively shorten the transportation length of the ion/electron and enhance the ECL intensity. More interestingly, after Bu_4NPF_6 as the co-reaction accelerator was added into the Py-sp^{2}c-CON/$S_2O_8^{2-}$ system, the ECL signal of the Py-sp^{2}c-CON/$S_2O_8^{2-}$/Bu_4NPF_6 system increased to 16559 a.u. (Figure 4A, curve e), which was about 2.03-fold higher than that of the Py-sp^{2}c-CON/$S_2O_8^{2-}$ system. Meanwhile, the ECL intensity of the Py-sp^{2}c-CON/$S_2O_8^{2-}$/Bu_4NPF_6 system was about 5.76, 24.31, and 190.33-fold higher than those of 3D bulk Py-sp^{2}c-COF/$S_2O_8^{2-}$, TFPPy/$S_2O_8^{2-}$ and imine-linked pyrene COF/$S_2O_8^{2-}$ systems. What is even more impressive is that the ECL intensity (Figure 4B) and the IR spectrum (Figure S2e) of Py-sp^{2}c-CON still remained unchanged after it was dispersed in water and stored at 4 °C for 6 months, which indicated that Py-sp^{2}c-CON possessed excellent ECL stability and water stability.

In addition, the ECL efficiency of Py-sp^{2}c-CON/$S_2O_8^{2-}$/Bu_4NPF_6, Py-sp^{2}c-CON/$S_2O_8^{2-}$, 3D bulk Py-sp^{2}c-COF/$S_2O_8^{2-}$, and TFPPy/$S_2O_8^{2-}$ systems were measured in PBS (the details are displayed in Supporting Information section 15). As seen from Table S2, the ECL efficiency of the Py-sp^{2}c-CON/$S_2O_8^{2-}$/Bu_4NPF_6 system was around 2.71, 3.70, and 14.58 times those of Py-sp^{2}c-CON/$S_2O_8^{2-}$, 3D bulk Py-sp^{2}c-COF/$S_2O_8^{2-}$, and TFPPy/$S_2O_8^{2-}$ systems. The above experiment results proved the 2D ultrathin Py-sp^{2}c-CON could be used as a new type of high-performance ECL emitter to construct ECL sensors, and Bu_4NPF_6 could be used as a co-reaction accelerator to enhance ECL intensity and efficiency of Py-sp^{2}c-CON.

Sensitivity of the Proposed ECL Biosensor. In order to assess the detection sensitivity of the proposed biosensor, the ECL responses of the sensor toward various concentrations of miRNA-21 were measured under the optimal experimental conditions (the optimization process is displayed in Supporting Information section 14). As we can see from Figure 5A, the

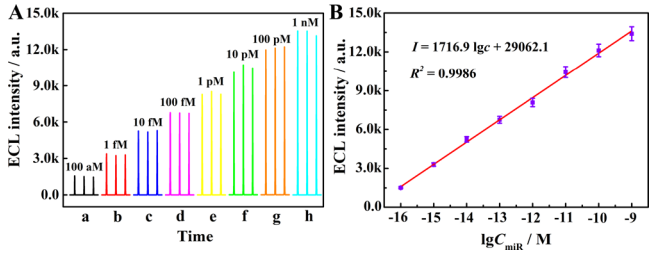

Figure 5. (A) ECL responses of the sensor toward various concentrations of miRNA-21. (B) Linear relationship between ECL intensity and the logarithm concentration of miRNA-21.

ECL response of the constructed biosensor enhanced accordingly as the concentration of miRNA-21 was changed from 100 aM to 1 nM. Meanwhile, an excellent linear relationship was achieved between the ECL intensities (I) and the logarithm values of miRNA-21 concentrations (lg c) with the regression equation I = 1716.9 lg c + 29062.1 and a correlation coefficient of 0.9986 (Figure 5B). The detection limit of the sensor was estimated to be 46 aM according to the standard 3σ rule. The proposed ECL biosensor displayed a higher sensitivity and lower detection limit in comparison with other reported sensors (Table 1), which proved the potential of this ECL sensor in biological detection.

Table 1. Comparison of this Work with Reported Works for miRNA-21 Detection

detection methods	linear range	detection limit	ref
fluorescence	1 fM to 10 pM	0.72 fM	51
fluorescence	10 to 500 fM	3.0 fM	52
electrochemistry	1 fM to 10 nM	0.31 fM	53
ECL	10 fM to 0.1 nM	6.6 fM	54
ECL	0.5 fM to 10 pM	0.17 fM	55
ECL	100 aM to 1 nM	46 aM	this work

Stability, Selectivity, and Reproducibility Analysis. As is known to all, the stability, selectivity, and reproducibility are crucial performances for the assessment of an ECL biosensor. The ECL biosensor was incubated with different concentrations of miRNA-21 (100 nM and 1 fM) and scanned continuously for 10 cycles to study its stability. As can be seen from Figure 6A, the ECL sensor showed steady signals with relative standard deviations (RSD) of 1.57 and 1.49%, respectively. The experiment results illustrated the ECL biosensor possessed outstanding stability.

To validate the selectivity of the ECL biosensor, five different miRNAs, including miRNA-155, miRNA-199a, miRNA-429, miRNA-141, and miRNA-144, were used as interfering substances. As shown in Figure 6B, target miRNA-21 (10 pM) caused a remarkable ECL response in comparison with that of the blank, while the miRNA-155, miRNA-199a, miRNA-429, miRNA-141, and miRNA-144 at a 100-fold concentration (1 nM) still exhibited negligible ECL responses. Furthermore, when 10 pM miRNA-21 was mixed with the aforementioned five interfering miRNAs, the ECL response exhibited little fluctuations compared with that of 10 pM miRNA-21. These results demonstrated the biosensor

https://dx.doi.org/10.1021/acs.analchem.0c04931
Anal. Chem. 2021, 93, 3258−3265

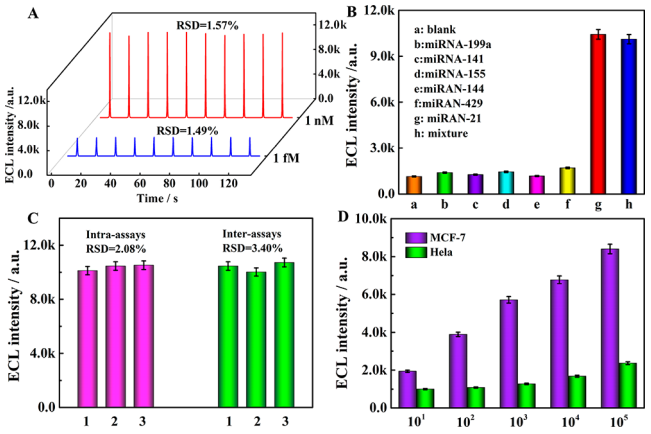

Figure 6. (A) Stability of the ECL sensor with miRNA-21 of different concentrations (1 fM and 1 nM) under 10 repetitive cyclic potential scans. (B) Selectivity of the constructed sensor toward other interfering miRNAs (1 nM). (C) Reproducibility of the constructed ECL biosensor when the miRNA-21 concentration was 10 pM. (D) Application of the constructed ECL sensor to detect miR-21 in Hela and MCF-7.

possessed superb selectivity and could be used for discriminating the target miRNA-21 over other control miRNAs.

As displayed in Figure 6C, the inter-assay (three tests were measured on three electrodes) and intra-assay (three tests were measured on the same electrode) experiments were performed to study the reproducibility of the proposed ECL biosensor. The RSD were 2.08% (n = 3) for intra-assays and 3.40% (n = 3) for inter-assays, respectively, suggesting the outstanding reproducibility of the ECL sensor.

Application. To assess the applicability of the constructed ECL sensor in cancer cell, the extracts of cervical cancer cells (Hela) and human breast cancer cells (MCF-7) were applied to execute an ECL assay with cell counts ranged from 10 to 10^5 cells. As revealed in Figure 6D, when the Hela concentrations were changed from 10 to 10^5 cells, the ECL responses slightly increased, which illustrated that the target miRNA-21 was lowly expressed in Hela cells. A significant ECL response increase was observed as the MCF-7 concentrations changing from 10 to 10^5 cells, which illustrated that the miRNA-21 was overexpressed in MCF-7 cells. The above results were in accordance with the reported work,[56] which demonstrated that the proposed ECL biosensor could be used for the detection of miRNA-21 in tumor cells.

CONCLUSIONS

In summary, a highly stable ultrathin Py-sp^{2}c-CON was directly used as a new type of ECL emitter to construct a supersensitive ECL sensor for the first time. Compared with a 3D bulk Py-sp^{2}c-COF, TFPPy, and an imine-linked pyrene COF, Py-sp^{2}c-CON exhibited higher ECL emission not only because Py-sp^{2}c-CON was constructed by the topological connection of pyrene luminophores and AIEgens, which efficiently decreased the ACQ effect and increased the loading amount of luminophores, but also because the ultrathin porous Py-sp^{2}c-CON could accelerate the migration of co-reactants, ions, and electrons, which made more internal luminophores to be electrochemically activated, thus improving the utilization ratio of ECL luminophores and enhancing ECL intensity. Furthermore, Bu_4NPF_6 as a co-reaction accelerator could further increase the ECL intensity of Py-sp^{2}c-CON. On the basis of the outstanding ECL performance of a Py-sp^{2}c-CON/$S_2O_8^{2-}$/Bu_4NPF_6 system and an Exo III-assisted target recycling amplification strategy, a novel ECL biosensor was successfully constructed to realize the ultrasensitive and highly selective determination of miRNA-21. In short, this work provided a new and hopeful strategy to design and prepare high-performance ECL materials, thereby initiating a brand-new chapter in the development of new types of ECL emitters and expanding the application of COFs in biological analysis.

ASSOCIATED CONTENT

Supporting Information

The Supporting Information is available free of charge at https://pubs.acs.org/doi/10.1021/acs.analchem.0c04931.

Materials and reagents; apparatus; synthesis of an imine-linked pyrene COF; the preparation of Pd NPs; Exo III-assisted target recycling amplification reaction; chemical structure of the Py-sp^{2}c-COF and imine-linked pyrene COF; infrared spectra of PNAD, TFPPy, Py-sp^{2}c-CON, and Py-sp^{2}c-COF; UV−vis absorption spectroscopy of the Py-sp^{2}c-COF and Py-sp^{2}c-CON; AFM of Py-sp^{2}c-CON; SEM images of Py-sp^{2}c-COF and the surface of electrodes; the ECL intensities of the TFPPy/$S_2O_8^{2-}$ system; ECL performance comparison of the Py-sp^{2}c-COF in different systems; the effect of Bu_4NPF_6 in the $[Ru(bpy)_3]^{2+}$/$S_2O_8^{2-}$/Bu_4NPF_6 system; ECL, CV, and EIS characterizations of the proposed biosensor; optimization of the experimental conditions, and ECL efficiency calculation (PDF)

AUTHOR INFORMATION

Corresponding Authors

Ruo Yuan − *Key Laboratory of Luminescence Analysis and Molecular Sensing (Southwest University), Ministry of Education, College of Chemistry and Chemical Engineering, Southwest University, Chongqing 400715, PR China;* orcid.org/0000-0003-3664-6236; Email: yuanruo@swu.edu.cn

Dong-Rong Xiao − *Key Laboratory of Luminescence Analysis and Molecular Sensing (Southwest University), Ministry of Education, College of Chemistry and Chemical Engineering, Southwest University, Chongqing 400715, PR China;* orcid.org/0000-0003-4610-1969; Phone: +86-23-68252360; Email: xiaodr98@swu.edu.cn; Fax: +86-23-68254000

Authors

Jin-Ling Zhang − *Key Laboratory of Luminescence Analysis and Molecular Sensing (Southwest University), Ministry of Education, College of Chemistry and Chemical Engineering, Southwest University, Chongqing 400715, PR China*

Yang Yang − *Key Laboratory of Luminescence Analysis and Molecular Sensing (Southwest University), Ministry of Education, College of Chemistry and Chemical Engineering, Southwest University, Chongqing 400715, PR China*

Wen-Bin Liang − *Key Laboratory of Luminescence Analysis and Molecular Sensing (Southwest University), Ministry of Education, College of Chemistry and Chemical Engineering, Southwest University, Chongqing 400715, PR China;* orcid.org/0000-0002-9086-4974

Li-Ying Yao − *Key Laboratory of Luminescence Analysis and Molecular Sensing (Southwest University), Ministry of*

https://dx.doi.org/10.1021/acs.analchem.0c04931
Anal. Chem. 2021, 93, 3258−3265

Education, College of Chemistry and Chemical Engineering, Southwest University, Chongqing 400715, PR China

Complete contact information is available at: https://pubs.acs.org/10.1021/acs.analchem.0c04931

Notes

The authors declare no competing financial interest.

■ ACKNOWLEDGMENTS

We would like to thank the NSFC (21571149) and Innovation Support Program for Chongqing Overseas Returnees (cx2017007 and cx2018026).

■ REFERENCES

(1) Lu, Z.; Liu, M.; Stribinskis, V.; Klinge, C. M.; Ramos, K. S.; Colburn, N. H.; Li, Y. *Oncogene* **2008**, *27*, 4373−4379.
(2) Medina, P. P.; Slack, F. J. *Cell Cycle* **2008**, *7*, 2485−2492.
(3) Yan, H.; Bhattarai, U.; Guo, Z.-F.; Liang, F.-S. *J. Am. Chem. Soc.* **2017**, *139*, 4987−4990.
(4) Wang, Z.; Ye, S.; Zhang, N.; Liu, X.; Wang, M. *Anal. Chem.* **2019**, *91*, 5043−5050.
(5) Xu, S.; Chang, Y.; Wu, Z.; Li, Y.; Yuan, R.; Chai, Y. *Biosens. Bioelectron.* **2020**, *149*, 111848.
(6) Bai, W.; Cui, A.; Liu, M.; Qiao, X.; Li, Y.; Wang, T. *Anal. Chem.* **2019**, *91*, 11840−11847.
(7) Zhang, H.; Huang, X.; Liu, J.; Liu, B. *Chem. Sci.* **2020**, *11*, 3812−3819.
(8) Liu, W.; Chen, A.; Li, S.; Peng, K.; Chai, Y.; Yuan, R. *Anal. Chem.* **2018**, *91*, 1516−1523.
(9) Liu, J.-L.; Zhang, J.-Q.; Tang, Z.-L.; Zhuo, Y.; Chai, Y.-Q.; Yuan, R. *Chem. Sci.* **2019**, *10*, 4497−4501.
(10) Dong, H.; Lei, J.; Ding, L.; Wen, Y.; Ju, H.; Zhang, X. *Chem. Rev.* **2013**, *113*, 6207−6233.
(11) Yao, L.-Y.; Yang, F.; Liang, W.-B.; Hu, G.-B.; Yang, Y.; Huang, W.; Yuan, R.; Xiao, D.-R. *Sens. Actuators, B* **2019**, *292*, 105−110.
(12) Yang, Y.; Hu, G.-B.; Liang, W.-B.; Yao, L.-Y.; Huang, W.; Yuan, R.; Xiao, D.-R. *Nanoscale* **2019**, *11*, 10056−10063.
(13) Huang, W.; Hu, G.-B.; Yao, L.-Y.; Yang, Y.; Liang, W.-B.; Yuan, R.; Xiao, D.-R. *Anal. Chem.* **2020**, *92*, 3380−3387.
(14) Zhou, J.; Li, Y.; Wang, W.; Tan, X.; Lu, Z.; Han, H. *Biosens. Bioelectron.* **2020**, *164*, 112332.
(15) Yao, L.-Y.; Yang, F.; Hu, G.-B.; Yang, Y.; Huang, W.; Liang, W.-B.; Yuan, R.; Xiao, D.-R. *Biosens. Bioelectron.* **2020**, *155*, 112099.
(16) Li, X.; Li, Z.; Lu, L.; Huang, L.; Xiang, L.; Shen, J.; Liu, S.; Xiao, D.-R. *Chem. − Eur. J.* **2017**, *23*, 10638−10643.
(17) Hu, G.-B.; Xiong, C.-Y.; Liang, W.-B.; Zeng, X.-S.; Xu, H.-L.; Yang, Y.; Yao, L.-Y.; Yuan, R.; Xiao, D.-R. *ACS Appl. Mater. Interfaces* **2018**, *10*, 15913−15919.
(18) Hu, G.-B.; Xiong, C.-Y.; Liang, W.-B.; Yang, Y.; Yao, L.-Y.; Huang, W.; Luo, W.; Yuan, R.; Xiao, D.-R. *Biosens. Bioelectron.* **2019**, *135*, 95−101.
(19) Yang, Y.; Hu, G.-B.; Liang, W.-B.; Yao, L.-Y.; Huang, W.; Zhang, Y.-J.; Zhang, J.-L.; Wang, J.-M.; Yuan, R.; Xiao, D.-R. *Nanoscale* **2020**, *12*, 5932−5941.
(20) Sasmal, H. S.; Halder, A.; Kunjattu, H. S.; Dey, K.; Nadol, A.; Ajithkumar, T. G.; Bedadur, P. R.; Banerjee, R. *J. Am. Chem. Soc.* **2019**, *141*, 20371−20379.
(21) Feng, X.; Ding, X.; Jiang, D. *Chem. Soc. Rev.* **2012**, *41*, 6010−6022.
(22) Liang, R. R.; A, R.-H.; Xu, S. Q.; Qi, Q. Y.; Zhao, X. *J. Am. Chem. Soc.* **2019**, *142*, 70−74.
(23) Li, R. L.; Flanders, N. C.; Evans, A. M.; Ji, W.; Castano, I.; Chen, L. X.; Gianneschi, N. C.; Dichtel, W. R. *Chem. Sci.* **2019**, *10*, 3796−3801.
(24) Mitra, S.; Sasmal, H. S.; Kundu, T.; Kandambeth, S.; Illath, K.; Díaz Díaz, D.; Banerjee, R. *J. Am. Chem. Soc.* **2017**, *139*, 4513−4520.
(25) Ying, Y.; Tong, M.; Ning, S.; Ravi, S. K.; Peh, S. B.; Tan, S. C.; Pennycook, S. J.; Zhao, D. *J. Am. Chem. Soc.* **2020**, *142*, 4472−4480.
(26) Guan, Q.; Zhou, L.-L.; Li, Y.-A.; Li, W.-Y.; Wang, S.; Song, C.; Dong, Y.-B. *ACS Nano* **2019**, *13*, 13304−13316.
(27) Gao, Q.; Li, X.; Ning, G.-H.; Leng, K.; Tian, B.; Liu, C.; Tang, W.; Xu, H.-S.; Loh, K. P. *Chem. Commun.* **2018**, *54*, 2349−2352.
(28) Wang, M.; Hu, M.; Liu, J.; Guo, C.; Peng, D.; Jia, Q.; He, L.; Zhang, Z.; Du, M. *Biosens. Bioelectron.* **2019**, *132*, 8−6.
(29) Chen, L.; He, L.; Ma, F.; Liu, W.; Wang, Y.; Silver, M. A.; Chen, L.; Zhu, L.; Gui, D.; Diwu, J.; Chai, Z.; Wang, S. *ACS Appl. Mater. Interfaces* **2018**, *10*, 15364−15368.
(30) Zeng, W.-J.; Wang, K.; Liang, W.-B.; Chai, Y.-Q.; Yuan, R.; Zhuo, Y. *Chem. Sci.* **2020**, *11*, 5410−5414.
(31) Dalapati, S.; Jin, E.; Addicoat, M.; Heine, T.; Jiang, D. *J. Am. Chem. Soc.* **2016**, *138*, 5797−5800.
(32) Ascherl, L.; Sick, T.; Margraf, J. T.; Lapidus, S. H.; Calik, M.; Hettstedt, C.; Karaghiosoff, K.; Döblinger, M.; Clark, T.; Chapman, K. W.; Auras, F.; Bein, T. *Nat. Chem.* **2016**, *8*, 310−316.
(33) Luo, J.; Xie, Z.; Lam, J. W. Y.; Cheng, L.; Chen, H.; Qiu, C.; Kwok, H. S.; Zhan, X.; Liu, Y.; Zhu, D.; Tang, B. Z. *Chem. Commun.* **2001**, 1740−1741.
(34) Tang, B. Z.; Zhan, X.; Yu, G.; Lee, P. P. S.; Liu, Y.; Zhu, D. *J. Mater. Chem.* **2001**, *11*, 2974−2978.
(35) Zhao, Q.; Li, K.; Chen, S.; Qin, A.; Ding, D.; Zhang, S.; Liu, Y.; Liu, B.; Sun, J. Z.; Tang, B. Z. *J. Mater. Chem.* **2012**, *22*, 15128−15135.
(36) Mei, J.; Leung, N. L. C.; Kwok, R. T. K.; Lam, J. W. Y.; Tang, B. Z. *Chem. Rev.* **2015**, *115*, 11718−11940.
(37) Zhao, Z.; Lu, P.; Lam, J. W. Y.; Wang, Z.; Chan, C. Y. K.; Sung, H. H. Y.; Williams, I. D.; Ma, Y.; Tang, B. Z. *Chem. Sci.* **2011**, *2*, 672−675.
(38) Chen, G.; Li, W.; Zhou, T.; Peng, Q.; Zhai, D.; Li, H.; Yuan, W. Z.; Zhang, Y.; Tang, B. Z. *Adv. Mater.* **2015**, *27*, 4496−4501.
(39) Li, Y.; Li, F.; Zhang, H.; Xie, Z.; Xie, W.; Xu, H.; Li, B.; Shen, F.; Ye, L.; Hanif, M.; Ma, D.; Ma, Y. *Chem. Commun.* **2007**, *3*, 231−233.
(40) Chandra, S.; Kandambeth, S.; Biswal, B. P.; Lukose, B.; Kunjir, S. M.; Chaudhary, M.; Babarao, R.; Heine, T.; Banerjee, R. *J. Am. Chem. Soc.* **2013**, *135*, 17853−17861.
(41) Jin, E.; Asada, M.; Xu, Q.; Dalapati, S.; Addicoat, M. A.; Brady, M. A.; Xu, H.; Nakamura, T.; Heine, T.; Chen, Q.; Jiang, D. *Science* **2017**, *357*, 673−676.
(42) Liang, W.-B.; Yang, M.-Z.; Zhuo, Y.; Zheng, Y.-N.; Xiong, C.-Y.; Chai, Y.-Q.; Yuan, R. *Chem. Sci.* **2016**, *7*, 7094−7100.
(43) Ma, M.-N.; Zhuo, Y.; Yuan, R.; Chai, Y.-Q. *Anal. Chem.* **2015**, *87*, 11389−11397.
(44) Zhang, R.; Zhong, X.; Chen, A.-Y.; Liu, J.-L.; Li, S.-K.; Chai, Y.-Q.; Zhuo, Y.; Yuan, R. *Anal. Chem.* **2019**, *91*, 3681−3686.
(45) Wei, X.; Zhu, M.-J.; Cheng, Z.; Lee, M.; Yan, H.; Lu, C.; Xu, J.-J. *Am. Ethnol.* **2019**, *131*, 3194−3198.
(46) Wang, F.; Lin, J.; Zhao, T.; Hu, D.; Wu, T.; Liu, Y. *J. Am. Chem. Soc.* **2016**, *138*, 7718−7724.
(47) Peng, H.; Huang, Z.; Deng, H.; Wu, W.; Huang, K.; Li, Z.; Chen, W.; Liu, J. *Angew. Chem., Int. Ed.* **2020**, *59*, 9982−9985.
(48) Yamase, T.; Takabayashi, N.; Kaji, M. *J. Chem. Soc., Dalton Trans.* **1984**, 793−799.
(49) Yang, C.; Yan, X.; Guo, S. *Chin. J. Inorg. Chem.* **1992**, *8*, 230−234.
(50) Yang, C.; Yan, X.; Guo, S. *Chin. J. Inorg. Chem.* **1992**, *8*, 441−443.
(51) Hu, J.; Liu, M.-h.; Zhang, C.-y. *Chem. Sci.* **2018**, *9*, 4258−4267.
(52) Xia, Y.; Wang, L.; Li, J.; Chen, X.; Lan, J.; Yan, A.; Lei, Y.; Yang, S.; Yang, H.; Chen, J. *Anal. Chem.* **2018**, *90*, 8969−8976.
(53) Zhang, X.; Yang, Z.; Chang, Y.; Qing, M.; Yuan, R.; Chai, Y. *Anal. Chem.* **2018**, *90*, 9538−9544.
(54) Zhang, P.; Jiang, J.; Yuan, R.; Zhuo, Y.; Chai, Y. *J. Am. Chem. Soc.* **2018**, *140*, 9361−9364.
(55) Peng, L.; Yuan, Y.; Fu, X.; Fu, A.; Zhang, P.; Chai, Y.; Gan, X.; Yuan, R. *Anal. Chem.* **2019**, *91*, 3239−3245.

(56) Si, M.-L.; Zhu, S.; Wu, H.; Lu, Z.; Wu, F.; Mo, Y.-Y. *Oncogene* **2007**, *26*, 2799−2803.

https://dx.doi.org/10.1021/acs.analchem.0c04931
Anal. Chem. 2021, 93, 3258−3265